Self-healing Atmospheric Plasma Sprayed $Mn_{1.0}Co_{1.9}Fe_{0.1}O_4$ Protective Interconnector Coatings for Solid Oxide Fuel Cells

Authors: Nikolas Grünwald[a], Doris Sebold[a], Yoo Jung Sohn[a], Norbert Heribert Menzler[a], Robert Vaßen[a]

[a]Forschungszentrum Jülich GmbH, Institute of Energy and Climate Research, Materials Synthesis and Processing (IEK-1), 52425 Jülich, Germany

Key Words:

- Solid oxide fuel cell interconnectors
- Mn1.0Co1.9Fe0.1O4 coatings
- Atmospheric plasma spraying
- Chromium protective coating
- Self-healing

Abstract:

Dense coatings on metallic interconnectors are necessary to suppress chromium poisoning of SOFC cathodes. Atmospherically plasma sprayed (APS) $Mn_{1.0}Co_{1.9}Fe_{0.1}O_4$ (MCF) protective layers demonstrated reduced chromium related degradation in laboratory and stack tests. Previous analyses revealed strong microstructural changes comparing the coating's as-sprayed and operated condition. This work concentrates on the layer-densification and crack-healing observed by annealing APS-MCF in air, which simulates the cathode operation conditions. The effect is described by a volume expansion induced by a phase transformation. Reducing conditions during the spray process lead to a deposition of the MCF in a metastable rock salt configuration. Annealing in air activates diffusion processes for a phase transformation to the low temperature stable spinel phase (T < 1050 °C). This transformation is connected to an oxygen incorporation which occurs at regions facing high oxygen partial pressures, as there are the sample surface, cracks and pore surfaces. Calculations reveal a volume expansion induced by the oxygen uptake which seals the cracks and densifies the coating. The process decelerates when the cracks are closed, as the gas route is blocked and further oxidation continues over solid state diffusion. The self-healing abilities of metastable APS coatings could be interesting for other applications.

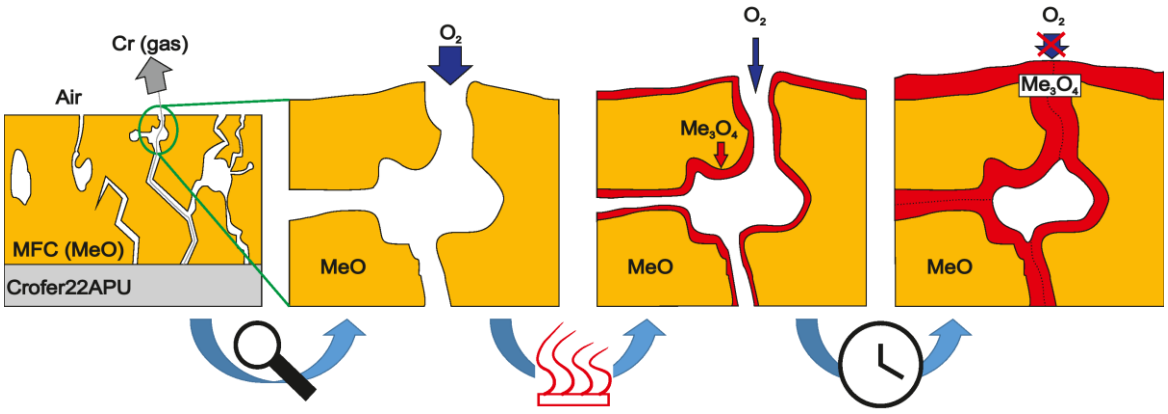

1 Introduction

In solid oxide fuel cell (SOFC) stacks interconnectors are used to establish electrical connection between single cells and separate the fuel and the oxidant gas. Chromium containing steels are widely used for this purpose, as they fulfill the interconnector's demands, such as high electrical conductivity, mechanical and chemical stability, and easy manufacturing. The disadvantage of this material arises from chromium oxides formed under operating conditions. Those Cr-containing oxides tend to evaporate at the high temperatures at which SOFCs operate. The chemical and electrochemical interaction of these chromium species at the cathode layer leads to strong degradation of commonly used cathode materials [1–5]. The strength of this chromium poisoning effect strongly depends on the steel's oxide layer that is formed under oxidizing (air side) conditions. Simple chromium base alloys build up Cr_2O_3 layers leading to a high chromium oxide partial pressure at elevated temperatures. Adjusting the steel's chemical composition influences the growing oxide scale and thereby changes the amount of released gaseous chromium species. Adding manganese as dopant material leads to the buildup of an outer chromium manganese oxide spinel layer covering the inner Cr_2O_3 layer. Measurements reveal a strong reduction of the chromium evaporation rate by improved passivation layers [3,6–8].

Applying a chromium protection layer between interconnector and cathode further decreases the chromium evaporation rate and thereby reduces the cathode degradation. For the manufacture of these layers different materials can be applied by several coating technologies, protecting the cathode in different ways. One possibility is applying porous coatings, e.g. wet powder sprayed (WPS) manganese oxides, which chemically bind volatile chromium species. Additionally it supports the buildup of the chromium manganese oxide spinel at the interconnector surface. Despite the reduced degradation rate, chromium can still be found at the cathode after long-term operation [9]. In terms of long-term stability, this kind of protection layer entails a limited chromium absorption capacity. Another possibility is

applying dense protective coatings that work in a different way by simply blocking the gas route for gaseous chromium oxides [5,10–12]. These kinds of coatings must provide the following properties: a) high electrical conductivity, b) high density, c) chemical stability under oxidizing (wet) environment up to about 900 °C, d) a thermal expansion coefficient that is adapted to the surrounding functional layers and the interconnector, e) adhesion on the interconnector's oxide scale, and f) low Cr-diffusion coefficient.

The effectiveness of dense chromium protective layers on metallic interconnects for solid oxide fuel cells induced a broad research on different material compositions applied by several coating techniques [5]. Hong et al. [13] achieved a densification of wet powder sprayed manganese-cobalt oxide coatings by reactive sintering. This cost efficient application technique faces the time and cost consuming sintering steps. Magnetron sputtering enables the deposition of very thin and dense protective layers [11] showing high conductivities but have to prove their stability in the long term and in stack tests. Further research on aerosol deposition [14], electrophoretic deposition [15,16], wet chemical methods [17] or several thermal spray techniques [12,18–20] revealed low chromium diffusion rates. Nevertheless, all protective coatings must exhibit minimum degradation for long-term operation within real stack tests. Atmospherically plasma sprayed (APS) $Mn_{1.0}Co_{1.9}Fe_{0.1}O_4$ (MCF) revealed its long-term stability and low chromium poisoning within real operation conditions. Fig. 1 shows the characteristic voltage-time behavior of two SOFC test stacks with different chromium protection coatings operated at Forschungszentrum Jülich [21]. The red line shows the recorded voltage of a still running stack with an operation time over 80,000 h, which keeps the world record in lifetime of planar SOFC systems. Its performance loss per 1,000 h, called average degradation rate, is about 0.6 %. The blue line illustrates the voltage curve of a four layer test-stack, which was shut down after more than 34,000 h of operation. The associated degradation rate of less than 0.3 % per 1,000 h is just half as the degradation rate of the other stack. The improved long-term stability is expected to originate from the difference between the integrated protection layers. In case of the stack

showing a higher degradation rate, a manganese oxide (MnO_x) layer was applied by WPS, while the interconnectors of the other stack are coated with an MCF protective coating applied by APS. In contrast to WPS-MnO_x layers, it is known that APS-MCF layers are rather dense [19]. From these two stacks it can be concluded that APS-MCF coatings are promising candidates for chromium protection layers (assuming that most of the additional degradation originates from the chromium-cathode interaction).

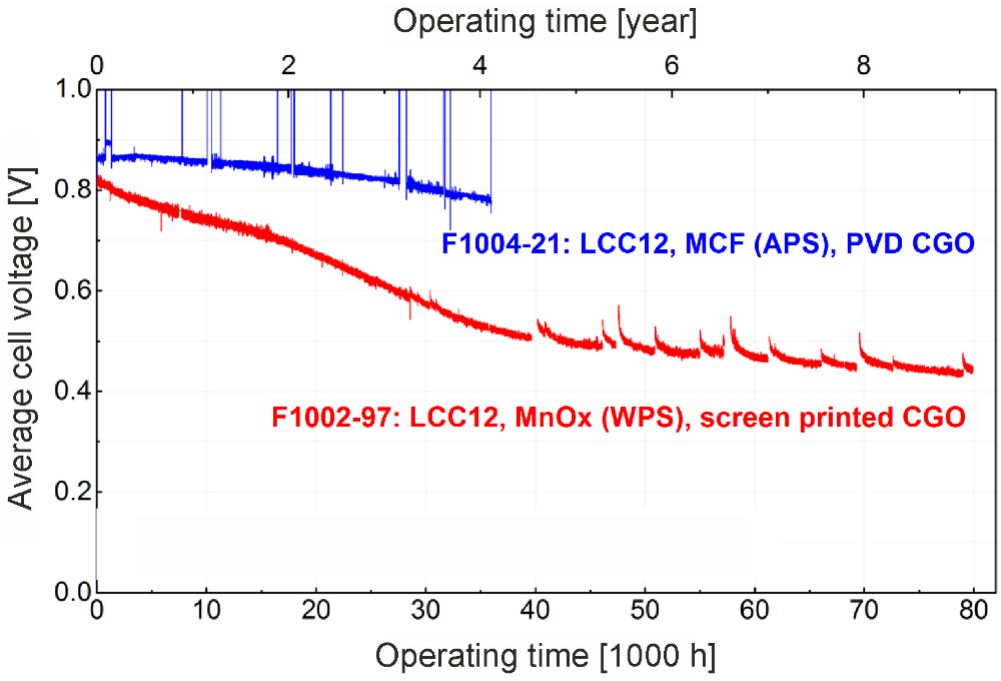

Fig. 1. Voltage degradation of two SOFC stacks operated at JÜLICH. Stack F1004-21 (blue) with APS-MCF protective coating and stack F1002-97 (red) with a WPS-MnOx coating. Modified after [21]. Reproduced with permission from J. Electrochem. Soc., 162 (9), F983 (2015). Copyright 2015, The Electrochemical Society.

Investigations of APS-MCF coated Crofer 22 APU interconnectors revealed a sufficient electrical conductivity, a good adhesion and remarkably low chromium evaporation rates [10,22,23]. Post-test analyses of stacks operated with APS-MCF layers and different studies of annealed thermally sprayed manganese-cobalt-(iron) oxide layers showed strong microstructural and phase changes between the as-sprayed and in air annealed condition [18,19,24,25]. A crack-healing effect during annealing is essential for the superior chromium-

restraint in stack operation. Vaßen et al. assumed this crack-healing and densification to arise from a phase transformation [19]. The present work concentrates on this phase transformation giving a full description of the crack-healing on the basis of theoretical calculations, enabling long-term predictions of these layers.

2 Experimental

The ferritic steel Crofer 22 APU (ThyssenKrupp VDM GmbH, Werdohl, Germany) [26] is used as substrate material with the dimensions 25*25*2.5 mm^3. To mimic more realistic SOFC stack conditions, the substrates were laser cut from original interconnector components with linear channel structure. Before coating, the substrates were sandblasted with F150 alumina particles (size 63-105 µm). As coating material, a manganese-cobalt-iron oxide powder in spinel configuration (H.C. Starck, Laufenburg, Germany) was chosen with the following chemical composition: 23.5 wt.% Mn, 47.6 wt.% Co, 2.4 wt.% Fe and 26.5 wt.% O. The associated stoichiometry is $Mn_{1.00}Co_{1.89}Fe_{0.10}O_{3.88}$. Particle sizes were measured to d_{10}=14 µm, d_{50}=27 µm and d_{90}=50 µm with a particle analyzer Horiba LA-950 V2 (Retsch Technology GmbH, Haan, Germany).

Atmospheric plasma spraying of the MCF powder was performed with a TriplexPro210 gun with a 9 mm nozzle within a multi coat facility (Oerlikon Metco, Wohlen, Switzerland). The parameters were set to a current of 500 A, a power of 49 kW and a plasma gas flow rate of 50 NLPM Argon and 4 NLPM Helium. To achieve a more homogenous layer thickness, three spray paths per coating were performed under different angles between substrate and plasma gun. The stand-off distance was set to 150 mm, leading to a layer thickness of 90 µm. High substrate temperatures during plasma spraying can lead to undesirable bending of real interconnectors. A high robot speed of 1500 mm s^{-1} reduces the thermal load, but leads to inhomogeneous feeding rates and thereby to varying layer thicknesses. The samples were heat treated under ambient atmosphere for 3 h at 500 °C, 100 h at 850 °C and 10,000 h at 700 °C. The annealing at 850 °C was chosen to simulate the stack sealing procedure in Jülich SOFCs, whereas the long-term annealing at 700 °C simulates standard SOFC operating conditions. The reason for choosing a heat treatment for 3 h at 500 °C is linked to the crack-healing phenomenon and will become clear in the result section.

Cross sections of the samples were obtained by embedding in epoxy, grinding and subsequent polishing with silica suspension. The specimens were sputtered with platinum in order to guarantee sufficient electrical conductivity for investigations with a scanning electron microscope (SEM) (Zeiss “Ultra55” with EDX from Oxford Instruments, INCAEnergy400). Porosity measurements were performed by image analyses based on seven SEM images at different locations within one sample. For phase analysis X-ray diffraction was performed using a D4 Endeavor (Bruker AXS GmbH, Karlsruhe, Germany). An essential property of chromium evaporation barriers is a high gas-tightness to minimize the amount of evaporating chromium species reaching the cathode in an SOFC stack. An air-leakage-tester Integra (Dr. Wiesner Steuerungstechnik GmbH, Remshalden, Germany) was used for measuring the air leakage rate of APS-MCF coatings. Porous tape cast Crofer 22 APU (manufactured in-house) served as substrates during the leakage-measurements guaranteeing a high leakage rate of the substrate and sufficient stability during the measurement. The samples were measured before and after annealing in air for 10 h at 500 °C and 100 h at 700 °C. Pure tape cast porous Crofer 22 APU were heat treated in the same furnace and leak-tested additionally to eliminate influences of the substrates.

Freestanding APS-MCF layers were required to prevent influences of any substrate material in case of wet chemical and thermogravimetric (TG) analyses. They were obtained by spraying MCF on a salt coated steel substrate and subsequent dissolving. For handling reasons these layers were sprayed with a thickness of 180 µm. Wet chemical analyses were performed to measure the chemical composition. To measure the ratio of Co:Mn:Fe, the samples were dissolved in Aqua Regia and measured with inductively coupled plasma optical emission spectrometry (ICP-OES). The oxygen content is determined by the inert gas fusion analysis (IFA) with a LECO TCH-600 analyzer (Leco Corporation, St. Joseph, USA). This method is based on the combustion of the sample in a graphite crucible under helium atmosphere. Oxygen contents are determined by the infrared absorption of emitting CO_2 products. Oxidation processes were observed by applying TG analyses with an STA 449 F1

Jupiter (NETZSCH-Gerätebau GmbH, Selb, Germany). Electron backscatter diffraction (EBSD) analyses were performed to visualize the local distribution of crystal phases within cross sectional samples. The measurements were performed with a NORD LYS II detector (Aztec (EDX and EBSD-System), Oxford Instruments, Abingdon, UK) integrated in an Zeiss Merlin SEM (Carl Zeiss Microscopy GmbH, Jena, Germany). Embedded freestanding APS-MCF layers were used to obtain extremely flat surfaces that are needed for high quality EBSD analyses.

3 Results

Electron microscopic images of cross sections of APS-MCF protective layers coated on Crofer 22 APU substrates are given in Fig. 2. The images are ordered from top to bottom with increasing annealing time and temperature. The different coating thicknesses in Fig. 2 a), c), e) and g) are related to variations in the powder feed rate during plasma spraying. Thus, no conclusions of the layer thickness evolution can be derived from the images. A sample in as-sprayed condition in Fig. 2 a) reveals a network of micro-cracks. This is even more pronounced on images with higher magnification on the right side (cf. Fig. 2 b). Porosity measurements, based on image analyses, determine a porosity of 12.4 ± 0.8 %. Fig. 2 c) and d) show a sample after an annealing for 3 h at 500 °C in ambient air. The micro-cracks location are still visible at higher magnification (Fig. 2 d), but seem to be filled with material, which is appearing bright in the SEM images. Additionally, the porosity is reduced to 2.4 ± 0.8 %. SEM images of 100 h annealed samples at 850 °C are shown in Fig. 2 e) and f). The micro-cracks are not visible even with higher magnification but the porosity increases to 6.3 ± 0.6 %. Cross-sectional images of a sample annealed for 10.000 h at 700 °C in air are depicted in Fig. 2 g) and h). The porosity was measured to 7.1 ± 1.3%. The signal for Cr was below the detection limit of EDX analyses in all measured samples. This indicates a low Cr diffusion and thereby an effective decrease of the Cr-poisoning in stack operation.

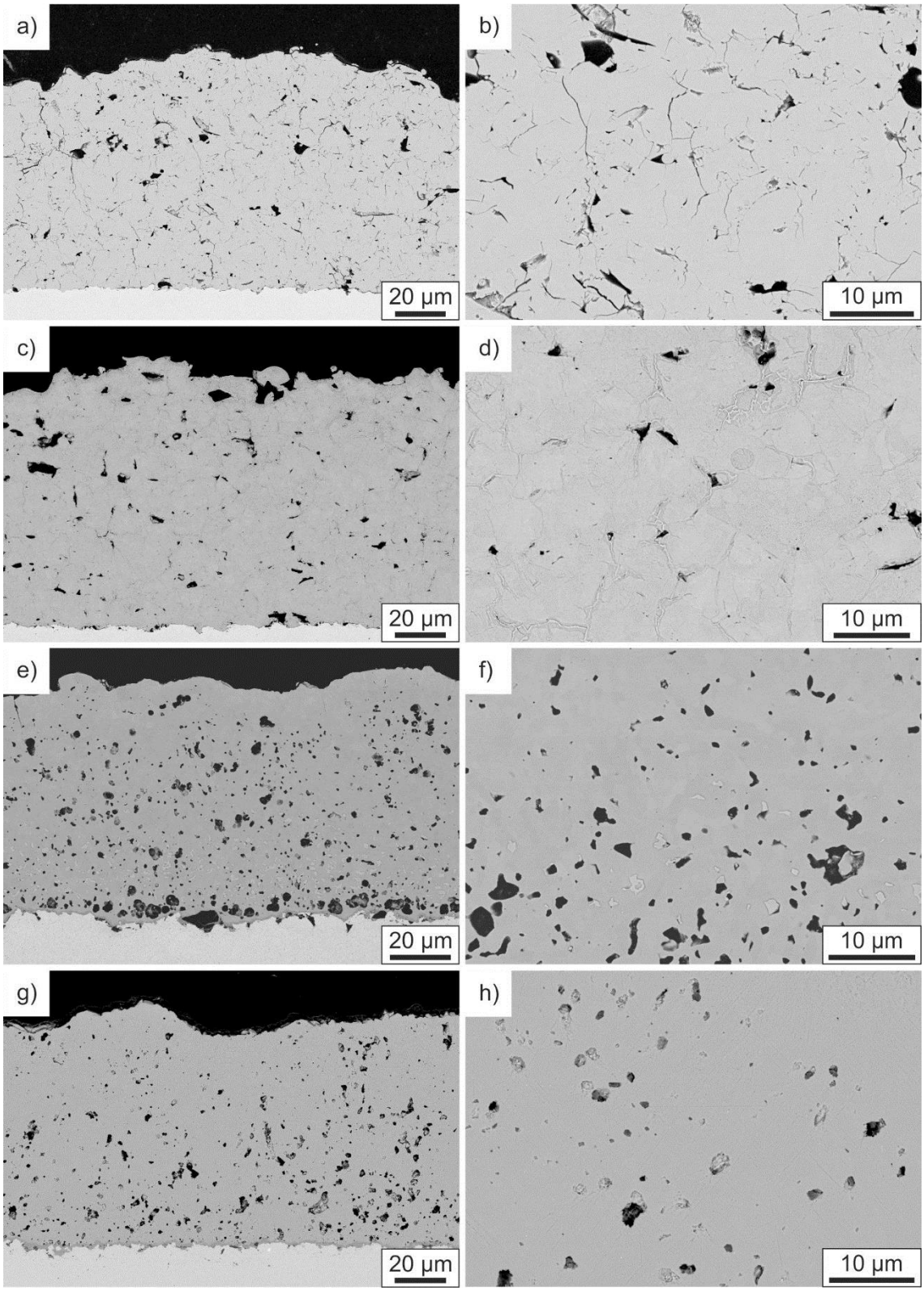

Fig. 2. SEM images of cross sections of APS-MCF coatings on Crofer 22 APU interconnectors. Part a & b depict the as-sprayed condition, c & d after annealing in air for 3 h at 500 °C, e & f after annealing in air for 100 h at 850 °C and g & h after annealing in air for 10.000 h at 700 °C. Left images with low and right images with high magnification.

Phase analyses by X-ray diffraction of the MCF powder used for APS, the as-sprayed coating, and the annealed samples are given in Fig. 3. The diffraction pattern of the powder confirms a cubic spinel phase ($Mn_{1.0}Co_{1.9}Fe_{0.1}O_4$) ([27] with adjusted lattice parameters), as declared by the producer H.C. Starck. The X-ray diffraction pattern of an as-sprayed coating indicate the presence of a cubic rock salt phase ((Mn,Co,Fe)O) ([28] with adjusted lattice parameters). After 3 h annealing at 500 °C in air, the following three phases could be identified: A rock salt configured (Mn,Co,Fe)O phase, as present in the as-sprayed coating; a spinel phase, similar to the diffraction pattern of the powder; and a mainly cobalt containing cubic spinel phase Co_3O_4 ([29] with adjusted lattice parameters). The diffraction pattern after 100 h annealing at 850 °C shows only reflections for the cobalt rich spinel configuration Co_3O_4. After annealing for 10,000 h at 700 °C, the initial spinel $(Mn,Co,Fe)_3O_4$ phase is recovered. A full profile refinement after the pawley method of each diffraction pattern is depicted in the supplementary.

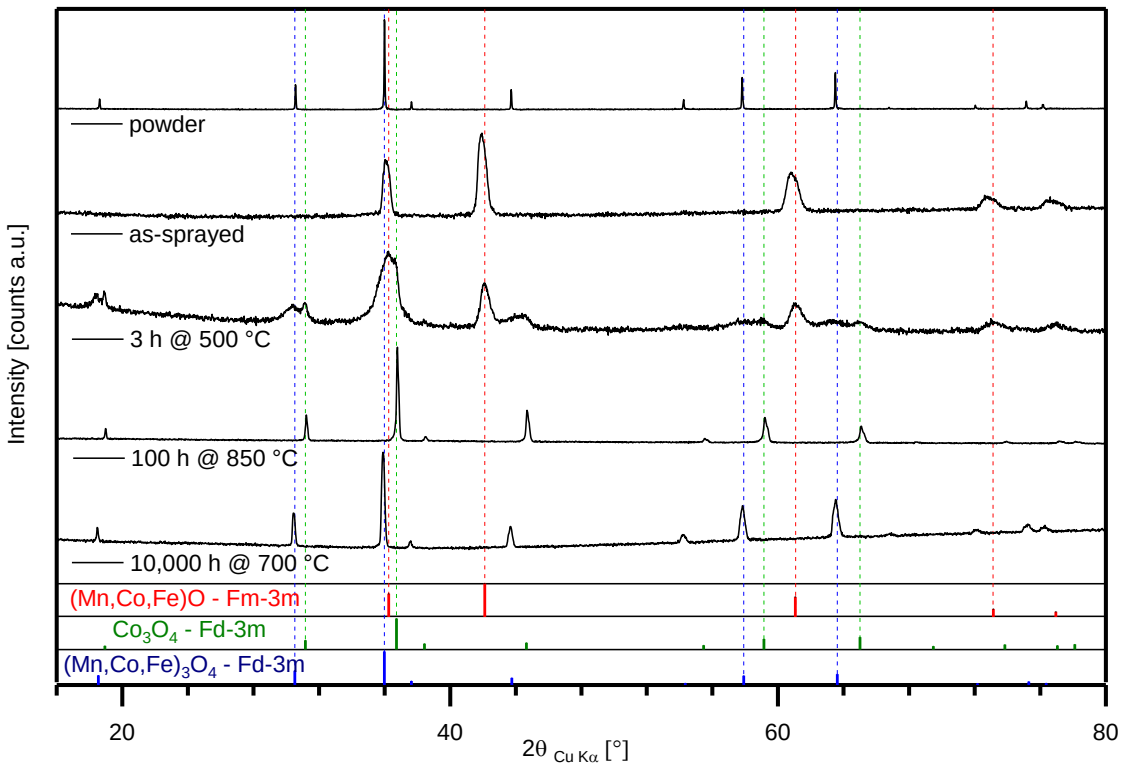

Fig. 3. X-ray diffraction patterns of MCF powder used for APS and APS-MCF coatings after different states of annealing. For each reference pattern the four reflections with the highest intensity are marked by dashed lines.

EBSD analyses were performed on cross sections of freestanding APS-MCF layers in the as-sprayed and 3 h at 500 °C annealed condition (Fig. 4). The forward scatter electron image of the as-sprayed coating in Fig. 4 a) reveals several micro-cracks that are visible as bright lines. The distribution of rock salt and spinel configured grains are visualized in the EBSD phase map in Fig. 4 b) by yellow and red areas, respectively. There is hardly any evidence for spinel configured material in the as-sprayed case. The forward scatter electron image and the EBSD phase map of a layer annealed for 3 h at 500 °C is shown in Fig. 4 c) and d), respectively. The phase map shows several areas of spinel configured material close to cracks and pore surfaces.

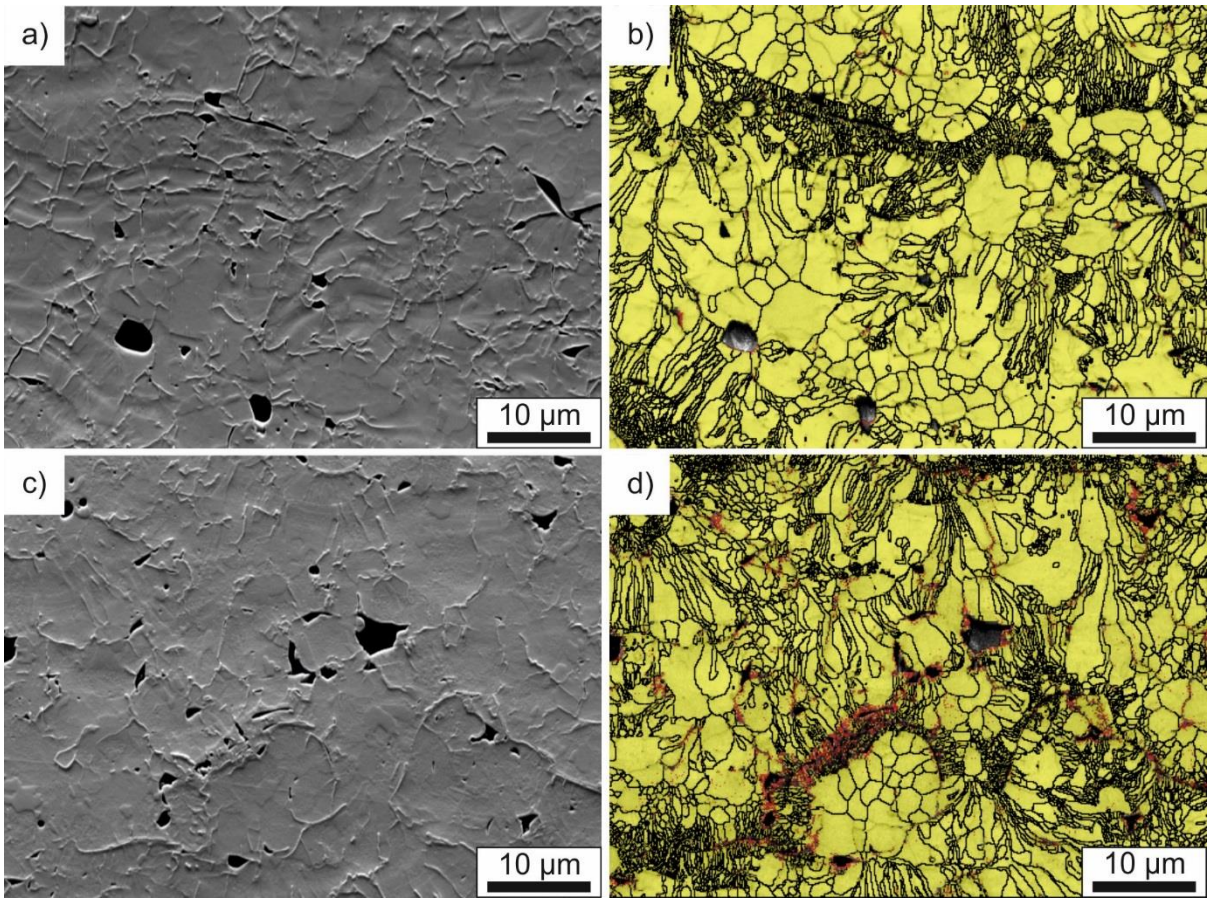

Fig. 4. Forward scatter electron image and EBSD phase map of an as-sprayed coating (a and b) and a layer annealed for 3 h at 500 °C (c and d). The rock salt phase (Fm-3m) is colored in yellow and the spinel phase (Fd-3m) in red.

Table 1 summarizes the results of ICP-OES and IFA measurements performed on MCF powder and freestanding APS-MCF coatings before and after annealing for 100 h at 850 °C in ambient air. The errors within the ICP-OES measurements, which is detecting the amount of cations, are quite high. The amount of oxygen is detected by IFA and reveals quite low errors. The last two rows of Table 1 give theoretically calculated ion concentrations of MCF in the rock salt and spinel configuration, assuming no changes in the cation ratio. In contrast to the measured amount of cations, the oxygen contents of the samples differ from each other. IFA measurements determined an oxygen loss of about 4.2 wt.% during the spray process. Annealing the layers for 100 h at 850 °C leads to an incorporation of oxygen in the same amount (within the error tolerance). These measured oxygen concentrations of the as sprayed and annealed sample are in agreement with the theoretical oxygen concentrations of the rock salt and spinel configured MCF, respectively.

	ICP-OES			IFA
	Mn [wt.%]	Co [wt.%]	Fe [wt.%]	O [wt.%]
Powder	23.5 ± 0.3	47.6 ± 0.2	2.42 ± 0.02	26.4 ± 0.7
As-sprayed	24.0 ± 1.0	48.0 ± 2.0	2.5 ± 0.1	22.2 ± 0.3
100 h at 850 °C	24.3 ± 0.9	47.0 ± 2.0	2.5 ± 0.1	26.7 ± 0.1
Rock salt phase	24.9	50.8	2.5	21.8
Spinel phase	23.2	47.3	2.4	27.1

Table 1. ICP-OES and IFA measurements of MCF powder and freestanding APS-MCF coatings before and after annealing for 100 h at 850 °C in air [19] and calculated mass fractions of MCF in rock salt and spinel configuration.

Fig. 5 shows a TG measurement of a freestanding APS-MCF layer in ambient atmosphere with a heating ramp of 5 °C min^{-1} to a temperature of 850 °C. After a dwell time of 50 h at 850 °C the sample is cooled to room temperature with 5 °C min^{-1}. The mass increase within the first 30 minutes and the mass decrease within the cooling phase are measurement

artifacts due to buoyancy. By calculating the extreme values of the TG signal, Fig. 5 can be divided in four sections. Part A (colored in red in Fig. 5) shows an increase of the mass uptake rate with increasing temperature after exceeding a temperature of 250 °C. The first maximum of the derivation of the TG-signal is at 400 °C marked by an arrow in Fig. 5. Between 400 °C and 550 °C, marked as section B in Fig. 5 (colored in blue), the TG-signal reveals a decrease of the mass uptake rate with increasing temperature. By rising the temperature from 550 °C to 850 °C, an increase of the mass uptake rate with increasing temperature is observable (section C in Fig. 5,colored in yellow). Section D (colored in green) marks the dwell time of 50 h at 850°C and shows an exponential behavior with an upper limit of 105.7 ± 0.5 wt.%. Subtracting the distortion by buoyancy results in a mass increase of 5.4 ± 0.5 wt.%. Even after an annealing of 50 h at 850°C the sample is not fully oxidized to the spinel phase, which is also confirmed by cross sectional SEM images (not shown here).

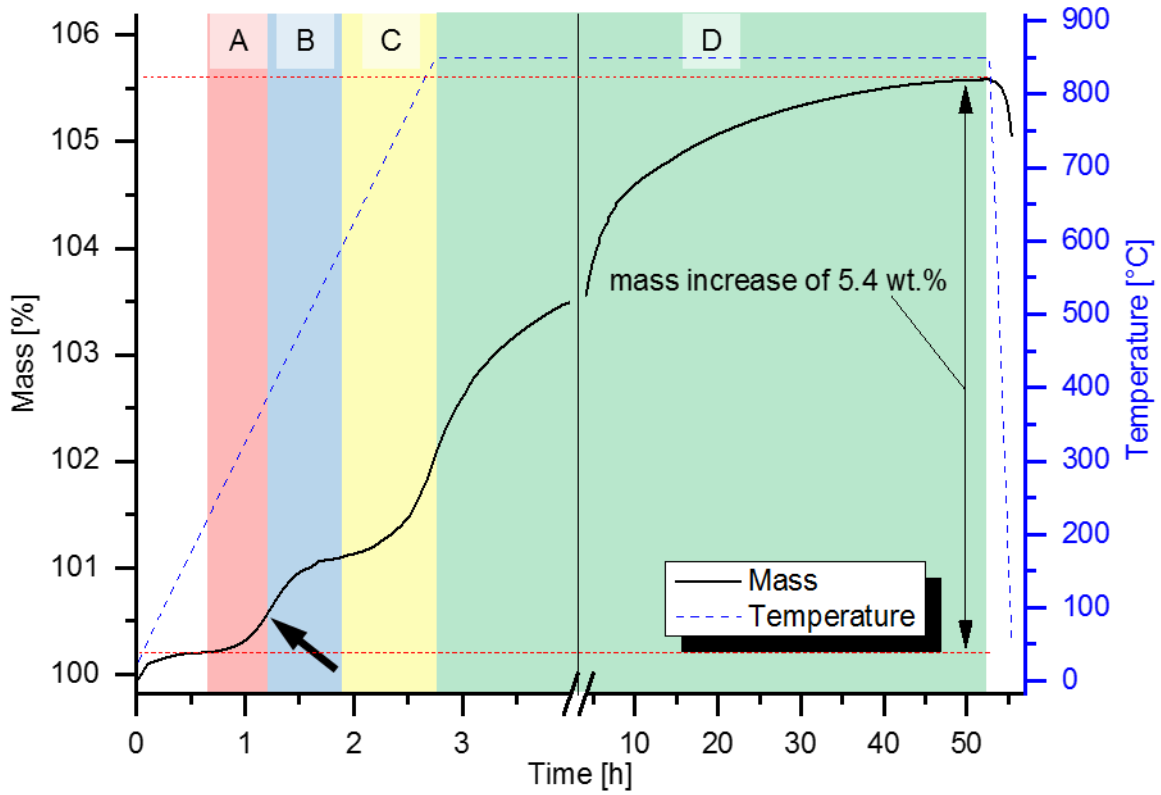

Fig. 5. Thermogravimetric measurement of a 160 µm thick freestanding APS-MCF layer under ambient atmosphere. The arrow marks a decrease of the mass uptake rate.

Air-leakage measurements of APS-MCF layers, sprayed on porous Crofer 22 APU substrates, are given in Table 2. Samples measured in the initial state reveal a high leakage rate that is decreasing strongly after an annealing procedure of 10 h at 500 °C. Increasing the annealing time and temperature to 100 h and 700 °C leads to a further decrease of the leakage rate, which is even lower, as the reference value for SOFC electrolytes [30]. Reference measurements were carried out on pure porous Crofer 22 APU substrates that were heat treated in the same furnace. They did not show the strong decrease of the gas leakage rate followed by the heat treatments. Measurements of samples annealed at higher temperatures have not been possible due to cracks in the substrate caused by strong corrosion of the Crofer 22 APU.

Heat treatment	Leakage rate at 1 bar [hPa dm^3 s^{-1} cm^{-2}]
None	$(9.3 \pm 7.8) * 10^{-1}$
10 h at 500 °C	$(4.4 \pm 2.4) * 10^{-4}$
100 h at 700 °C	$(8.93 \pm 0.28) * 10^{-6}$
SOFC electrolyte (reference)	$2.30 * 10^{-4}$
Pure porous Crofer 22 APU substrates annealed for 100 h at 700 °C	$(6.3 \pm 3.1) * 10^{-1}$

Table 2. Air leakage measurements performed on APS-MCF coated porous Crofer 22 APU substrates. The leakage tolerance limit for SOFC electrolytes is given as reference [30].

4 Discussion

All three annealing phenomena of APS-MCF coatings, as there are crack-healing, porosity decrease and increased gas-tightness, are linked to each other and are based on a phase transformation. To understand the phase transformation of the coatings during annealing, it is crucial to know the development of the crystal phase from the powder to the as-sprayed coating. The X-ray diffraction patterns in Fig. 3 exhibit a transformation from a spinel configured powder $(Mn,Co,Fe)_3O_4$ to a rock salt configuration (Mn,Co,Fe)O that is present in the as-sprayed coating. The phase diagram of manganese-cobalt oxide in [31] indicates that the rock salt phase is only stable at high temperatures. Below 1050 °C the spinel configuration is the stable phase in case of $Mn_1Co_2O_x$. Although the phase diagram describes the phase stability of manganese-cobalt oxide without the influence of iron, it gives a good approximation for the investigated material. The deposition of MCF in a metastable rock salt configuration has its origin in the fast cooling of molten powder particles on the cold substrate during plasma spraying [19,24,32].

Subsequent annealing of APS-MCF in air can activate diffusion processes for the phase transformation back to the low temperature stable spinel configuration. The phase transformation can be described by the following simplified chemical reaction equation (according to the phase diagram in [31]):

$$3\ (Mn,Co,Fe)O + \frac{1}{2}O_2 \rightarrow (Mn,Co,Fe)_3O_4$$

This reaction implies an oxygen uptake during annealing, which is validated by the IFA results given in Table 1 and the TG measurements shown in Fig. 5. The oxygen uptake causes a volume expansion, which can be calculated from the measured lattice parameters. Taking the number of cations as constant, the volume per cation and unit cell leads to a theoretical volume expansion of $\Delta V\ V^{-1}$=21.1 % (Table 3).

	Fm-3m $(Mn,Co,Fe)O_3$	Fd-3m $(Mn,Co,Fe)_3O_4$
Measured lattice parameter (XRD) [Å]	4.28	8.29
→ Unit cell volume [$Å^3$]	78.40	569.72
Cations per unit cell	4	24
Calculated volume per cation [$Å^3$]	**19.60**	**23.74**

Table 3. Calculation of the theoretical volume of one unit cell of MCF in the rock salt and in the spinel phase.

This chemical reaction occurs preferably at regions with a high oxygen partial pressure. Within APS-MCF coatings these areas are the coating's surface, as well as pore surfaces and the micro-cracks in the coating's bulk, as illustrated by Fig. 6 a) to c). The EBSD phase map in Fig. 4 shows that the phase transformation occurs preferably in these regions. The reaction takes place also in the sample's bulk, as quenching cracks in APS-MCF coatings reveal open porosity [33,34]. Within the TG measurements this initial oxidation is observable as mass increase between 250 °C and 400 °C marked as red colored region A in Fig. 5. The volume expansion, induced by the phase transformation, leads to crack-healing observed in the SEM micrographs in Fig. 2. Thereby, the porosity is decreasing from 12.4 % of the as-sprayed condition to 2.4 % after annealing for 3 h at 500 °C. After closing of the micro-cracks, oxygen cannot reach the coating's bulk via gas phase diffusion, as illustrated by Fig. 6 d). Further oxidation has to proceed via solid state diffusion. Thereby, the oxidation speed is strongly reduced, which is visible as a decrease of the mass uptake rate in the TG measurement in Fig. 5 (blue marked area B). The diffusion processes dominating further oxidation of the material lead to a demixing and a porosity increase to 6.3 % by annealing 100 h at 850 °C. Due to the complexity of these reaction they are beyond (and are not in) the scope of this article. The temperature of this untypical oxidation behavior starts at about 400 °C and is marked with an arrow in Fig. 5. The results of the air leakage test in Table 2 also

confirm a decreasing in gas permeability due to the closed micro-cracks. Regarding the coating's use as chromium evaporation layer for SOFCs, the densification diminishes the amount of chromium reaching the cathode via the gas phase. Other degradation processes occurring with low chromium partial pressures on the cathode side are described in [35].

The self-healing ability of APS-MCF depends on the amount of rock salt phase in the coating's bulk. The major part of the oxidation is happening after the cracks are closed, thus driven by solid state diffusion. In the TG measurement this is visualized by the green area D in Fig. 5. The total oxygen uptake of 4.5 ± 0.7 wt.% measured by IFA and 5.4 ± 0.5 wt.% measured by TG analyses is in good agreement with the theoretically calculated value of 5.3 wt.%. The velocity of diffusion processes is strongly temperature dependent and can be observed within the yellow marked area C in Fig. 5. Thus, the self-healing ability of APS-MCF can be extended in time by decreasing the annealing temperature. This unique self-healing property of plasma sprayed metastable coatings could also be interesting for other applications operating at temperatures between 450 °C and 850 °C.

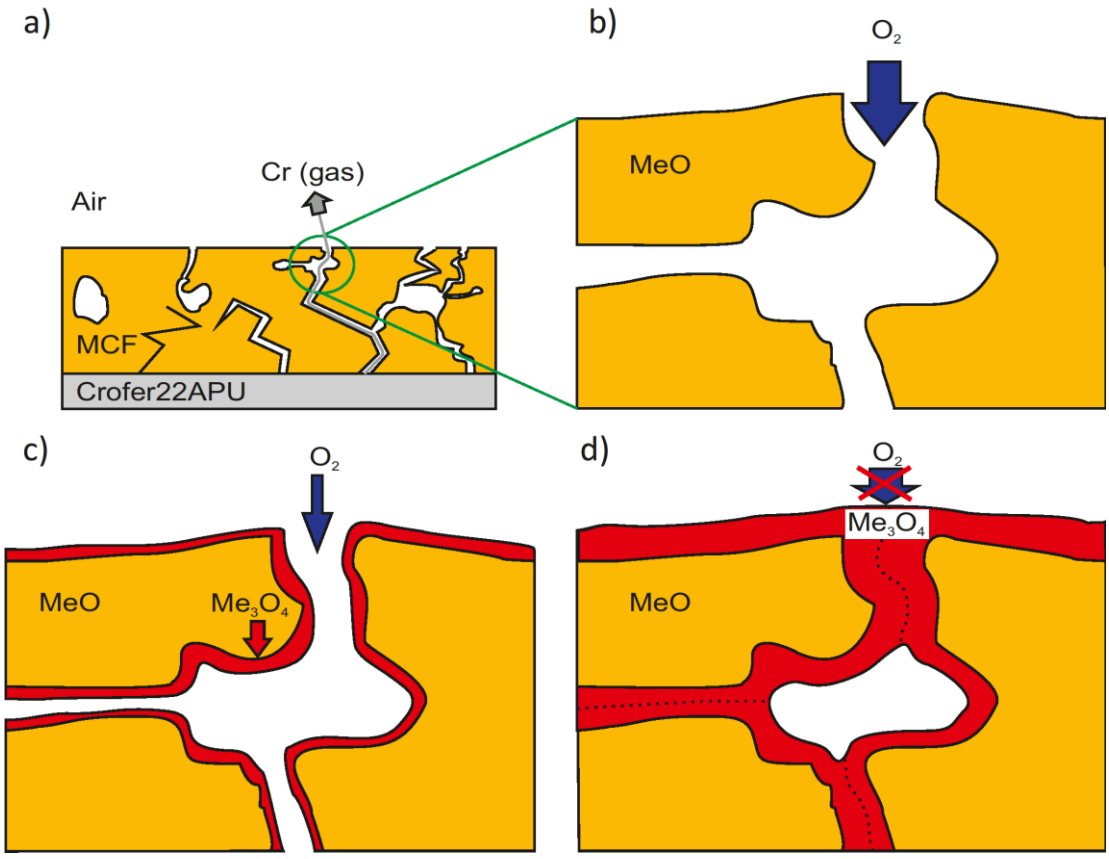

Fig. 6. Schematic drawing of the crack-healing process. By annealing fresh sprayed APS-MCF in air, the MeO (Me = $Mn_{1.0}Co_{1.9}Fe_{0.1}$) rock salt phase transforms into the spinel configuration Me_3O_4. This oxidation leads to a volume expansion, which takes place at the MCF surfaces (c). Oxygen cannot penetrate to the bulk over the gas phase after the cracks are closed (d).

5 Conclusion

MCF protective layers have been applied on Crofer 22 APU interconnector substrates by atmospheric plasma spraying. A network of micro-cracks can be observed in the as-sprayed condition, which has a negative influence on the coating's gas tightness and thereby the chromium-restraint (Fig. 6 a). Phase analyses by XRD revealed the crystal structure to be in a metastable rock salt configuration (Mn,Co,Fe)O due to quenching during thermal spraying. By annealing APS-MCF in air, which simulates SOFC operation conditions on the cathode side, the MCF transforms to the low temperature stable spinel phase $(Mn,Co,Fe)_3O_4$. The phase transformation is accompanied by an oxygen uptake leading to a volume expansion at surfaces facing a high oxygen partial pressure (Fig. 6 b and c). The densification of the layer continues until the cracks are closed and further oxidation is limited to solid state diffusion (Fig. 6 d). By blocking the gas routes, the coating efficiently blocks volatile chromium species reaching the cathode material and thereby diminish SOFC degradation. No pretreatment is necessary to achieve these unique self-healing properties. This self-healing ability of plasma sprayed metastable coatings could also be interesting for other applications.

6 Glossary

APS	atmospheric plasma spraying
EBSD	electron backscatter diffraction
EDX	energy dispersive X-ray spectroscopy
ICP-OES	inductively coupled plasma optical emission spectroscopy
IFA	inert gas fusion analysis
MCF	$Mn_{1.0}Co_{1.9}Fe_{0.1}O_4$
MnO_x	manganese oxide
SEM	scanning electron microscopy
SOFC	solid oxide fuel cell
TG	thermogravimetry
WPS	wet powder spraying
XRD	X-ray diffraction

7 Supplementary data

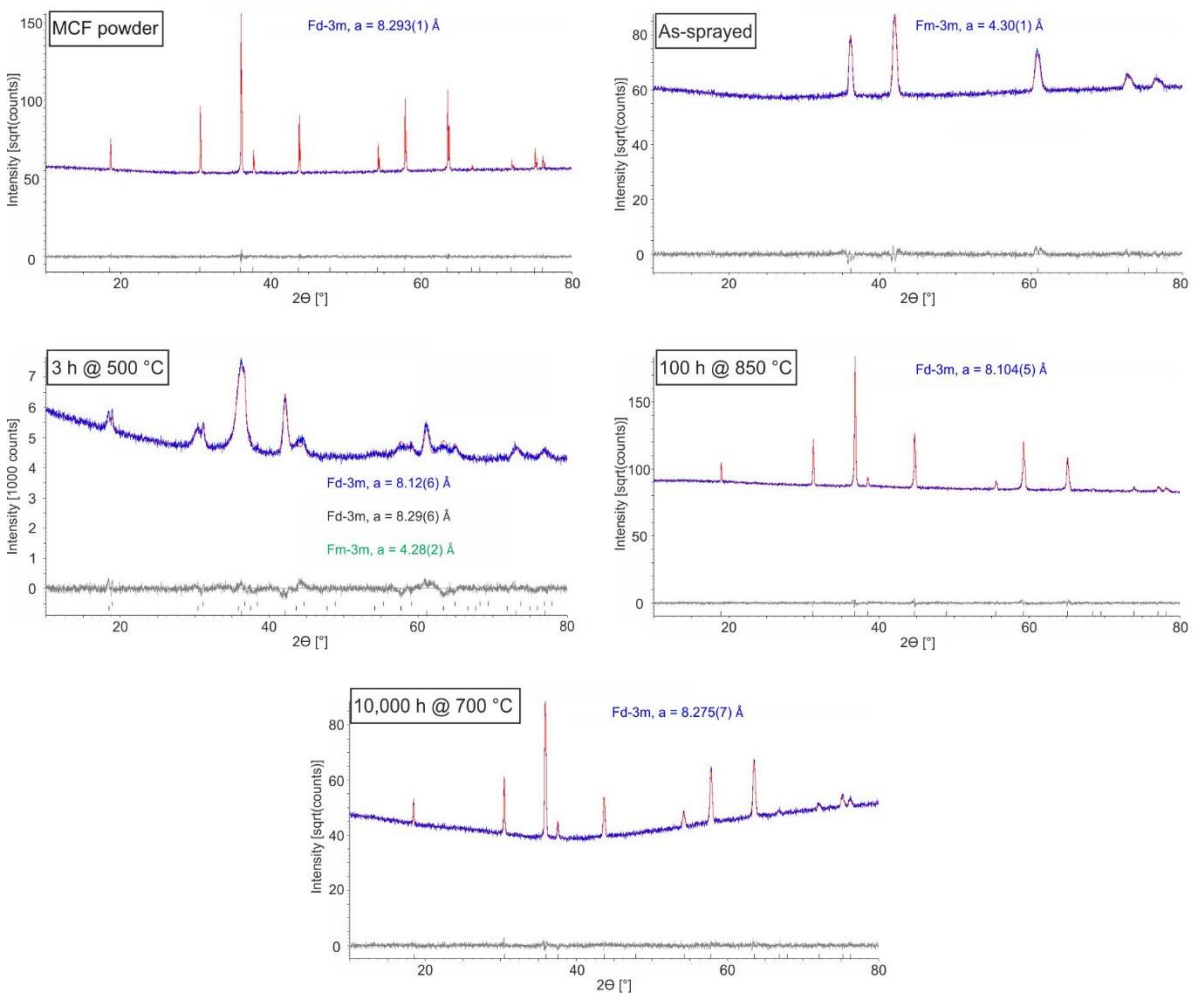

Supplementary data 1: X-ray diffraction patterns and full profile refinements after the pawley method of the MCF powder used for APS and APS-MCF coatings after different states of annealing. The blue line marks the measured XRD-signal, the red line the fitted profile and the gray line the deviation between these two. The space groups used for the refinements and the lattice parameters are given in each diagram. In case of the diffraction pattern of the sample annealed for 3 h at 500 °C, the space groups are color coded and ordered as the reference pattern below the diffraction pattern.

Acknowledgement:

The authors would like to acknowledge the support of Mr. Frank Kurze and Mrs. Marie-Theres Gerhards, Forschungszentrum Jülich, Institute of Energy and Climate Research: Materials Synthesis and Processing (IEK-1), for manufacturing MCF coatings and for performing TG measurements, respectively. The authors acknowledge Dr. Egbert Wessel, Forschungszentrum Jülich, Institute of Energy and Climate Research: Microstructure and Properties of Materials (IEK-2) for conducting the EBSD measurements and Prof. Ludger Blum, Forschungszentrum Jülich, Institute of Energy and Climate Research: Electrochemical Process Engineering (IEK-3) for providing data of test stacks. For performing wet chemical analyses the authors would like to thank Volker Nischwitz, Forschungszentrum Jülich, Central Institute for Engineering, Electronics and Analytics (ZEA-3). The project "Verbundvorhaben SOFC Degradation" (proposal number 03SF0494A) was funded by the German Federal Ministry of Education and Research (BMBF).

8 References

[1] S. Taniguchi, M. Kadowaki, H. Kawamura, T. Yasuo, Y. Akiyama, Y. Miyake, T. Saitoh, Journal of Power Sources 55 (1995) 73–79.

[2] S. BADWAL, R. DELLER, K. FOGER, Y. RAMPRAKASH, J. ZHANG, Solid State Ionics 99 (1997) 297–310.

[3] E. Konysheva, H. Penkalla, E. Wessel, J. Mertens, U. Seeling, L. Singheiser, K. Hilpert, Journal of the Electrochemical Society 153 (2006) A765.

[4] A. Neumann, N.H. Menzler, I. Vinke, H. Lippert, in: 216th ECS Meeting, October 4 - October 9, 2009, pp. 2889–2898.

[5] N. Shaigan, W. Qu, D.G. Ivey, W. Chen, Journal of Power Sources 195 (2010) 1529–1542.

[6] P. Huczkowski, V. Shemet, J. Piron-Abellan, L. Singheiser, W.J. Quadakkers, N. Christiansen, Materials and Corrosion 55 (2004) 825–830.

[7] W.J. Quadakkers, J. Piron-Abellan, V. Shemet, L. Singheiser, Mat. at High Temp. 20 (2003) 115–127.

[8] M. Stanislowski, J. Froitzheim, L. Niewolak, W.J. Quadakkers, K. Hilpert, T. Markus, L. Singheiser, Journal of Power Sources 164 (2007) 578–589.

[9] T. Kiefer, Entwicklung neuer Schutz- und Kontaktierungsschichten für Hochtemperatur-Brennstoffzellen, Forschungszentrum Jülich, 2007.

[10] L. Blum, L.G. de Haart, J. Malzbender, N.H. Menzler, J. Remmel, R. Steinberger-Wilckens, Journal of Power Sources 241 (2013) 477–485.

[11] Q. Fu, F. Tietz, D. Sebold, E. Wessel, H.-P. Buchkremer, Corrosion Science 54 (2012) 68–76.

[12] J. Puranen, J. Laakso, M. Honkanen, S. Heinonen, M. Kylmälahti, S. Lugowski, T.W. Coyle, O. Kesler, P. Vuoristo, International Journal of Hydrogen Energy 40 (2015) 6216–6227.

[13] J.-E. Hong, M. Bianco, J. van herle, R. Steinberger-Wilckens, ECS Transactions 68 (2015) 1581–1587.

[14] J.-J. Choi, J. Ryu, B.-D. Hahn, W.-H. Yoon, B.-K. Lee, D.-S. Park, J Mater Sci 44 (2009) 843–848.

[15] A. Das Sharma, J. Mukhopadhyay, R.N. Basu, in: ECS Transactions (2011), pp. 2509–2517.

[16] W. Huang, S. Gopalan, U.B. Pal, S. Basu, in: ECS Transactions, ECS, 2008, pp. 405–411.

[17] S. Molin, P. Jasinski, L. Mikkelsen, W. Zhang, M. Chen, P.V. Hendriksen, Journal of Power Sources 336 (2016) 408–418.

[18] S.J. Han, Z. Pala, S. Sampath, Journal of Power Sources 304 (2016) 234–243.

[19] R. Vaßen, N. Grünwald, D. Marcano, N.H. Menzler, R. Mücke, D. Sebold, Y.J. Sohn, O. Guillon, Surface and Coatings Technology 291 (2016) 115–122.

[20] J. Puranen, J. Laakso, M. Kylmälahti, P. Vuoristo, J Therm Spray Tech 22 (2013) 622–630.

[21] L. Blum, P. Batfalsky, Q. Fang, L.G.J. de Haart, J. Malzbender, N. Margaritis, N.H. Menzler, R. Peters, J. Electrochem. Soc. 162 (2015) F1199-F1205.

[22] T. Kiefer, M. Zahid, F. Tietz, D. Stöver, H.-R. Zerfass (Eds.), Electrical conductivity and thermal expansion coefficientes of spinels in the series MnCo2-xFexO4 for application as a protective layer in SOFC, 2005.

[23] D. Udomsilp, D. Roehrens, N.H. Menzler, R. Conradt, O. Guillon, ECS Transactions 68 (2015) 751–756.

[24] E. Saoutieff, G. Bertrand, M. Zahid, L. Gautier, in: 216th ECS Meeting, October 4 - October 9, 2009, pp. 1397–1402.

[25] J. Puranen, M. Pihlatie, J. Lagerbom, G. Bolelli, J. Laakso, L. Hyvärinen, M. Kylmälahti, O. Himanen, J. Kiviaho, L. Lusvarghi, P. Vuoristo, International Journal of Hydrogen Energy 39 (2014) 17284–17294.

[26] Crofer 22 APU Werkstoffdatenblatt Nr. 4146, ThyssenKrupp VDM, 2010, http://www.vdm-metals.com/fileadmin/user_upload/Downloads/Data_Sheets/Datenblatt_VDM_Crofer_22_APU.pdf.

[27] J.L. Gautier, S. Barbato, J. Brenet, COMPTES RENDUS DE L ACADEMIE DES SCIENCES SERIE II 294 (1982) 427–430.

[28] S. SASAKI, K. FUJINO, Y. TAKÉUCHI, Proceedings of the Japan Academy, Series B 55 (1979) 43–48.

[29] J.P. Picard, G. Baud, J.P. Besse, R. Chevalier, Journal of the Less Common Metals 75 (1980) 99–104.

[30] P. Ried, C. Lorenz, A. Brönstrup, T. Graule, N.H. Menzler, W. Sitte, P. Holtappels, Journal of the European Ceramic Society 28 (2008) 1801–1808.

[31] E. AUKRUST, A. MUAN, J American Ceramic Society 46 (1963) 511.

[32] O. Thomann, M. Pihlatie, M. Rautanen, O. Himanen, J. Lagerbom, M. Mäkinen, T. Varis, T. Suhonen, J. Kiviaho, J Therm Spray Tech 22 (2013) 631–639.

[33] R. Vaßen, F. Traeger, D. Stöver, Journal of Thermal Spray Technology 13 (2004) 396–404.

[34] R. Vaßen, D. Hathiramani, J. Mertens, V. Haanappel, I.C. Vinke, Surface and Coatings Technology 202 (2007) 499–508.

[35] N.H. Menzler, P. Batfalsky, A. Beez, L. Blum, S.-M. Gross-Barsnick, L. Niewolak, W.J. Quadakkers, R. Vassen (Eds.), Post-test analysis of a solid oxide fuel cell stack operated for 35,000h, 2016.